

Medical Image Compression Approach Based on Image Resizing, Digital Watermarking and Lossless Compression

Hedi Amri^{1,2} · Ali Khalfallah² · Malek Gargouri² · Naïma Nebhani^{1,2} · Jean-Christophe Lapayre¹ · Mohamed-Salim Bouhleb²

Received: 22 February 2016 / Revised: 1 June 2016 / Accepted: 8 June 2016 / Published online: 23 July 2016
© Springer Science+Business Media New York 2016

Abstract The computerization of images have been important for different medical applications. Nevertheless, the huge volume of medical images can rapidly saturate transmission especially in telemedicine field and may encumber storage systems in case of local saving. Data compression represents the most used solution to deal with this problem. Indeed, it can minimize the data space and may reduce both the time of data transfer and bandwidth consumption. In this context, we have proposed new approaches, which combined image reduction and expansion techniques, digital watermarking and lossless compression standards such as JPEG-LS (JLS) and TIFF formats. We named these compression methods wREPro.TIFF (watermarked Reduction/Expansion Protocol combined with TIFF format) and wREPro.JLS (wREPro combined with

JPEG-LS format). The results of comparative experiments show that we have provided significant improvements over the well-known JPEG image compression standard. Indeed, our proposed compression algorithms have ensured a better preservation of the image quality notably for high compression ratios.

Keywords Image compression · Reduction · Expansion · Watermarking · Archiving · Transmission · Telemedicine · JPEG-LS · TIFF

1 Introduction

The explosive growth in the use of Internet has made it an attractive medium for data exchange in many areas as telemedicine, mobile military applications, e-learning, etc. Nowadays, hospitals and clinical environments are quickly moving toward computerization. This fact allows digitalization, processing, stocking and transmission of medical images to deal with the fast growing data [1, 2].

Modern medical imaging have produced a great amount of data that can rapidly saturate transmission and storage systems [3, 4]. To surmount this problem, a data compression have usually been essential [5, 6]. In this context, several medical image compression techniques have been developed to reduce the image volume such as Fractal coding methods [7], Region of Interest Coding Techniques [8, 9], Lossless dynamic and adaptive compression [10], low-complexity compression [11] and genetic algorithms [12]. However, JPEG [13], JPEG 2000 [14, 15], TIFF and JPEG-LS (JLS) [16] have remained among the widespread methods used as standards since they provided better performance in image compression.

We note that these techniques are based on coding algorithms applied on transformed images to frequency or

✉ Hedi Amri
hedi.amri@femto-st.fr

Ali Khalfallah
ali.khalfallah@enetcom.mu.tn

Malek Gargouri
malek.gargouri@setit.rnu.tn

Naïma Nebhani
naima.nebhani@univ-fcomte.fr

Jean-Christophe Lapayre
jc.lapayre@femto-st.fr

Mohamed-Salim Bouhleb
medsalim.bouhleb@enis.rnu.tn

¹ FEMTO-ST/DISC Institute (UMR CNRS 6174), Computer Science for Complex Systems Dept DISC, University of Franche-Comté, Besançon, France

² Research Unit: Sciences and Technologies of Image and Telecommunications, Higher Institute of Biotechnology, University of Sfax, Sfax, Tunisia

multiresolution domains [17, 18]. Moreover, some medical applications tolerate the use of lossy compression as long as the compressed image does not yield to erroneous diagnosis [19].

In this work, we propose a new medical image compression approach that combined the image size reduction and a lossless image compression method [20]. To minimize the image size, we utilized the square-square mesh method. We exploited the digital watermarking to embed in each pixel of the decimated image the code of its best enlargement approach [21]. The used image expansion techniques were “zero-padding”, “nearest-neighbor interpolation”, “cubic interpolation” and “transformed B-Spline”.

To further decrease the data volume to be archived or transmitted, we suggested compressing the reduced watermarked image [22, 23]. Hence, we chose to use encoding lossless compression methods such as TIFF and JLS. Before displaying the image on the screen, the user had to decompress the image, select the enlargement approach by extracting and decoding the inserted information and use it to enlarge the image. We named this process watermarked Reduction / Expansion Protocol (wREPro) [24] combined with lossless image compression.

The rest of this paper is organized as follows. Section 2 presents some techniques of expansion, reduction and watermarking [25]. In section 3, we detail our proposed approaches. In Section 4, we reveal the results of the application of our methods on various types of medical images. The conclusion is presented in Section 5.

2 Used Methods

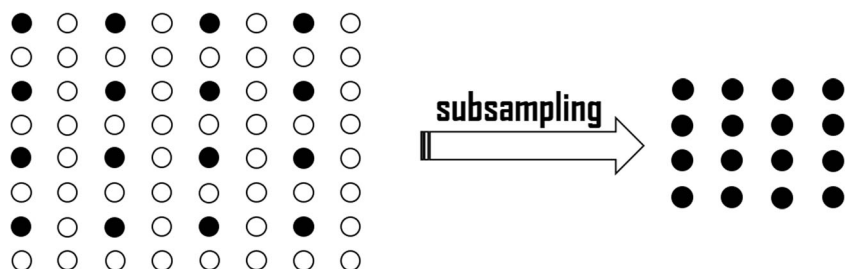
2.1 Square-Square Mesh Decimation

The reduction of an image by a factor of 2 was carried out horizontally and vertically. It removed basically a sample out of two in each direction [26]. Thus, the function of spatial decimation could be simply expressed by Eq. 1:

$$\begin{cases} d_s(x,y) = 1 & \text{when } x \text{ and } y \text{ are even} \\ d_s(x,y) = 0 & \text{otherwise} \end{cases} \quad (1)$$

According to Fig. 1, this decimation type kept each pixel with even coordinates (x,y) and eliminated other pixels.

Figure 1 Image Reduction by a factor of 2 using Square-Square Mesh.



2.2 Expansion Methods

Several algorithms have been developed and allowed researchers to expand images. To achieve this goal, we have chosen to exploit mainly the following four expansion techniques: Zero-padding, Nearest-neighbor interpolation, Cubic interpolation and Transformed B-spline interpolation.

To simplify the presentation of these methods, we focused only on the one-dimensional interpolation that was performed with a convolution product in the spatial domain. It could be easily extended on two dimensions benefiting from the separability of the 2D interpolation functions.

2.2.1 Zero-Padding Technique

The zero-padding method emanates from the spectral preservation concept. Indeed, the image is transformed into the frequency domain by the Discrete Fourier Transform (DFT). Then, the spectrum is expanded by appending zero-valued samples in the added high frequencies. Finally, we apply the inverse Discrete Fourier Transform (DFT⁻¹) on the last result to obtain the spatial representation of the magnified image [27]. The mathematical description of this process in the spatial domain is presented by the Eqs. 2 and 3.

$$g(x) = \sum_{m=-\frac{aN}{2}}^{\frac{aN}{2}-1} f^{\uparrow a}(m) \cdot h\left(\frac{x-m}{a}\right) = f^{\uparrow a} * h\left(\frac{x}{a}\right) \quad (2)$$

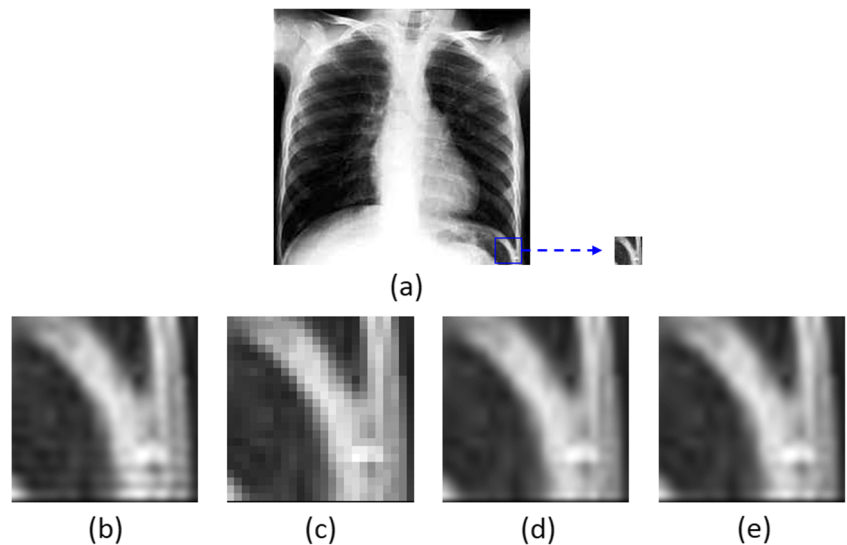
Where g is the expanded signal, h is the cardinal sine function and N denotes the number of samples of f . The function $f^{\uparrow a}$ is obtained by appending $a-1$ zeros between the samples of f as explained in Eq. 3.

$$\left(-\frac{aN}{2} \leq m < \frac{aN}{2}\right) \begin{cases} f^{\uparrow a}(m) = f\left(\frac{m}{a}\right) & \text{when } \frac{m}{a} \text{ is an integer} \\ f^{\uparrow a}(m) = 0 & \text{otherwise} \end{cases} \quad (3)$$

2.2.2 The Nearest-Neighbor Interpolation

This technique represents the simplest and the fastest expansion function. It involves a duplication of the original pixels so as to obtain a new enlarged image. In fact, to each new pixel is assigned the value of the nearest pixel. This method also

Figure 2 Visual effects of image enlargement by a factor equal to 64. **a** Sample of the original image, **b** Expansion by Zero-padding, **c** Expansion by the nearest neighbor technique, **d** Expansion by cubic interpolation, **e** Expansion by B-Spline function.



applies the Eq. 1 while changing the interpolation function h as depicted in Eq. 4 [28].

$$\begin{cases} h(x) = 1 & \text{if } |x| \leq \frac{1}{2} \\ h(x) = 0 & \text{otherwise} \end{cases} \quad (4)$$

2.2.3 The Cubic Interpolation

In this method, each four closest pixels are used to compute the value of the new pixel by applying a polynomial of degree three. In order to reduce this solution spaces, various constraints are imposed on these polynomials such as symmetry around zero, continuity and first continuous derivative at the connection points [29]. Thus, we obtain a cubic interpolation function h as described in Eq. 5, then it is used in Eq. 2 (expansion equation).

$$\begin{cases} h(x) = \frac{3}{2}|x^3| - \frac{5}{2}x^3 + 1 & \text{when } |x| \leq 1 \\ h(x) = -\frac{1}{2}|x^3| + \frac{5}{2}x^2 - 4|x| + 2 & \text{when } \frac{1}{2} \leq |x| \leq \frac{3}{2} \\ h(x) = 0 & \text{otherwise} \end{cases} \quad (5)$$

2.2.4 Interpolation with B-Spline Function

This technique uses all the original image pixels to calculate the values of the expanded image pixels. The continuous B-

spline function is obtained by applying n times a self-convolution of the rectangle function defined in Eq. 4 and called here « β^0 » [30]:

$$\beta^n(x) = \beta^{n-1} * \beta^0(x) = \beta^0 * \dots * \beta^0(x) \quad (6)$$

The interpolation by the B-spline function is realized in two steps. In the first one, we make a direct transformed B-Spline [31]. In the second phase, we carry out an indirect transformed B-Spline.

The B-spline coefficients “ $C(u)$ ” are determined by a direct linear filtering operation known as B-spline transformation and are depicted in Eq. 7.

$$C(u) = F(u) \cdot \beta^n(u)^{-1} \quad (7)$$

where the function $F = \text{TFD}(f)$ is the frequency spectrum of the original signal.

The simplest approach to expand $f(x)$ by a factor a from its B-spline representation starts with the insertion of $a-1$ zeros between the B-Spline “ $C(x)$ ” coefficients. Then, the result is interpolated with the B-Spline “ B^n ” function n which is dilated by the factor a as explained in Eq. 8.

$$g(x) = c^{\uparrow a} * \beta_a^n(x) \quad (8)$$

where $\beta_a^n(k) = \beta^n(\frac{k}{a})$ [28] and $c^{\uparrow a}$ is defined analogously to Eq. 3.

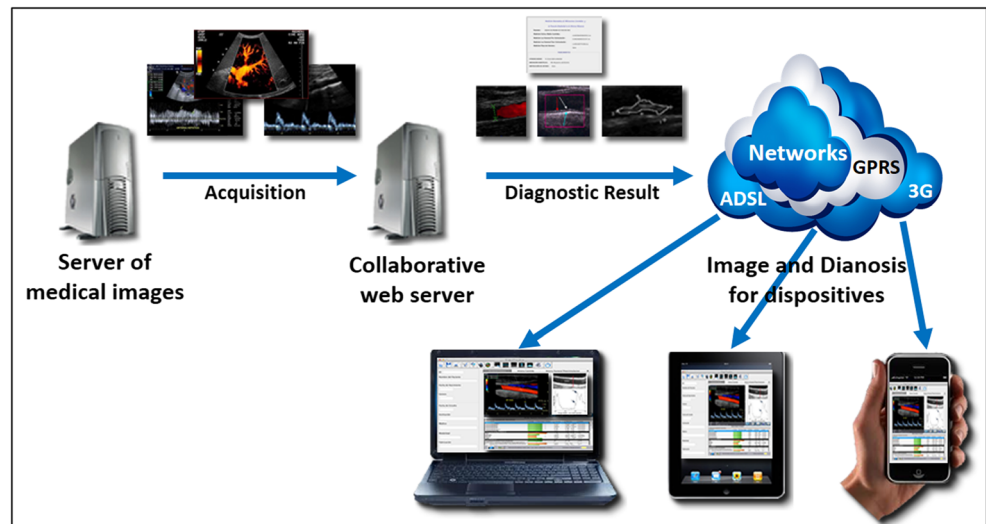
Table 1 Assessments of the expansion techniques applied on MR images.

	RE ₁	RE ₂	RE ₃	RE ₄
PSNR _{avg} (dB)	46,79	46,17	37,32	46,21
SSIM _{avg}	0,9974	0,9965	0,9833	0,9968

Table 2 Evaluations of the expansion techniques applied on CR images.

	RE ₁	RE ₂	RE ₃	RE ₄
PSNR _{avg} (dB)	34,08	34,17	41,77	33,1
SSIM _{avg}	0,9954	0,9956	0,9873	0,9919

Figure 3 Image transmission process using REPro.



2.2.5 Evaluation of Image Expansion Methods

In this section, we show the effect of the described expansion methods on one image. This sample was expanded by a factor equal to 64 as described in Fig. 2a.

In this example, although we note a normal magnification by the zero-padding approach far from the image borders, we notice the presence of artifacts (undulations) in these borders (Fig. 2b.). The observed undulations are mainly caused due to a filtering (on–off controller), which yields to spectral discontinuities.

Using the nearest neighbor technique, these undulations were removed but image pixelation appeared (Fig. 2c.). The detected flaw was due to the allocation of nearest-neighbor values to those of new added pixels. As for the expanded image by cubic interpolation (Fig. 2d.), it presented a significant reduction in the image pixelation and an absence of ripples. Furthermore, this image shows some blur due to the dependence of the estimated pixel value to the neighboring pixels values.

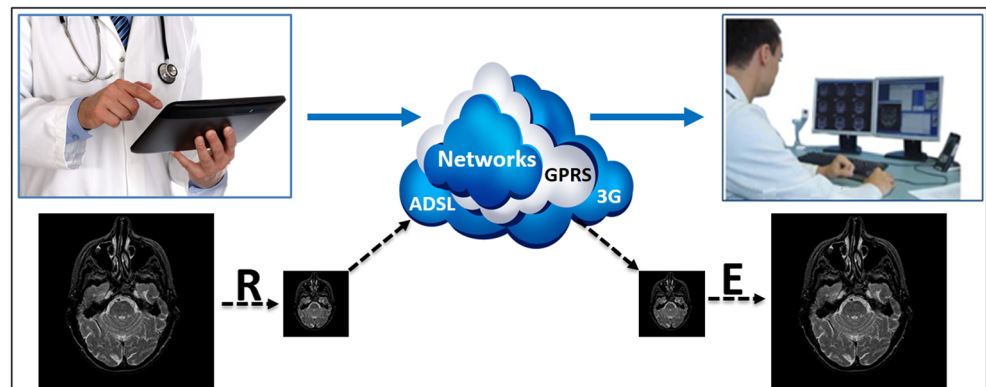
Comparing the B-Spline interpolation function with the previous techniques, we note that it decreased the image blurring and the pixelation effect and removed the defects of corrugations (Fig. 2e.) [24]. However, we notice an increase of the execution time [32].

For a more objective comparison, we will use PSNR [33] and SSIM [34] to quantify the error introduced by the expansion techniques applied on reduced images. This comparison is performed on 30 MR images and 30 CR images reduced (reduction factor equal to 2) by decimation square-square grid (R) then enlarged magnified with 4 four technical magnification (expansion factor equal to 2) Namely B-spline interpolation function (E1), cubic interpolation (E2), nearest-neighbor interpolation (E3) and zero-padding (E4). The result of this quantitative comparison are shown in Tables 1 and 2 in terms of average PSNR and average SSIM between original images and their reduced then enlarged counterparts. The analysis of these results shows that B-spline interpolation function ensures the best quality image preservation for MR images while the nearest-neighbor interpolation seems the best enlargement technique of the reduced CR images.

2.3 Image Watermarking

The watermarking allows the insertion of a digital data into an image. This embedded signal can be simply a set of information as binary or real numbers [35, 36]. The watermarking was originally used as a tool for copyright

Figure 4 REPro Protocol.



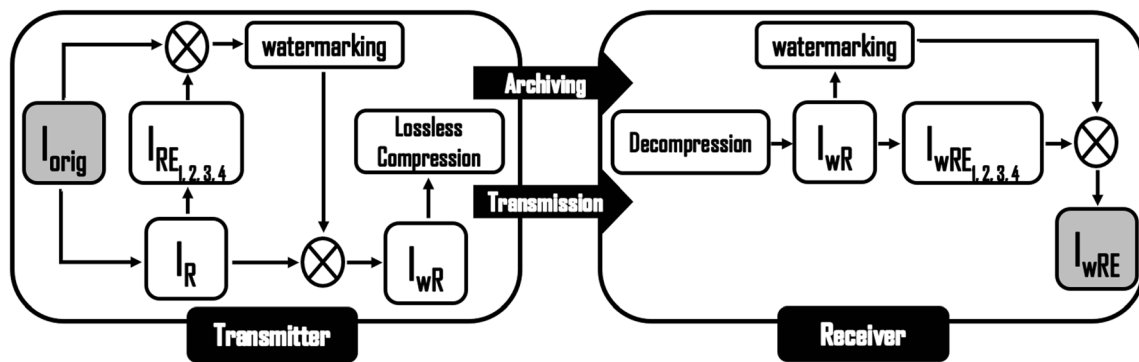


Figure 5 wREPro Protocol.

protection [37] to be later involved in various application fields such as medical secrecy preservation, integrity control, and digital fingerprint.

This method consists of signature insertion and extraction (or detection).

In the insertion phase, the marking of a document can be realized in one of the possible information presentations. It can be carried out by substituting some of the image elements by the signature values or by combining the elements of data to embed with the chosen image components as described in Eq. 9.

$$I_w = F(T(I), W(b_0, b_1, \dots, b_{n-1}), \alpha) \tag{9}$$

Where I_w represents the watermarked image, I is the original image and $T(I)$ is one of its spatial, frequency or multiresolution representation. $b_{i=1:n}$ are the elements of the signature W having n as length, α represents the visibility coefficient of the watermark insertion and F denotes one of the available insertion functions in [37].

In the extraction phase, three types of watermarking can be distinguished according to the available information. Indeed, this method is called blind when the watermark detector requires only the marked image, whereas it is considered as semi-blind [38] when the detector needs both the marked image and the embedded signal [39]. However, we may need both the original and marked images and the inserted signature. This kind of watermarking is called non-blind [36].

Thus, we can note that watermarking performances (robustness, insertion capacity, imperceptibility, complexity and security) are imposed by the desired purposes of watermarking application.

Table 3 Assessments of the reduction-expansion techniques applied on MR images.

	RE ₁	RE ₂	RE ₃	RE ₄	RE _w
PSNR _{avg} (dB)	46,79	46,17	37,32	46,21	50,6
SSIM _{avg}	0,9974	0,9965	0,9833	0,9968	0,9989

3 A New Transmission Protocol “wREPro” Combined with Lossless Image Compression

3.1 The Fundamentals of the Protocol “REPro”

Medical images have usually large sizes. Hence, their transmission on the network consumes a great part of the available bandwidth. To remedy this problem, we have proposed the Reduction / Expansion Protocol (REPro) [24]. On the one hand, this method aims to reduce the size of the image before its sending. On the other hand, this transmitted image can be enlarged to fit the screen that will display it (Fig. 3). This feature increases the visual comfort and facilitates the diagnosis [40, 41].

However, the explained compression process based on both reduction and expansion (Fig. 4) in the image spatial domain could not be done without degrading the quality of the reconstructed image after its reception. Therefore, it was necessary to develop an algorithm that identified the best expansion techniques ensuring better conformity between the original and reproduced images.

3.2 Watermarked REPro (wREPro) Combined with JPEG-LS and TIFF Formats

During the image reduction using the square-square decimation, one pixel out of four was preserved, whereas, during the image expansion, one pixel was known and three had to be estimated (Fig. 2).

Thus, the image could be divided into 2x2 blocks in which one pixel was known and three were unknown. The previous section listed four expansion techniques that can be used to

Table 4 Evaluations of the reduction-expansion techniques applied on CR images.

	RE ₁	RE ₂	RE ₃	RE ₄	RE _w
PSNR _{avg} (dB)	34,08	34,17	41,77	33,1	51,25
SSIM _{avg}	0,9954	0,9956	0,9973	0,9919	0,9992

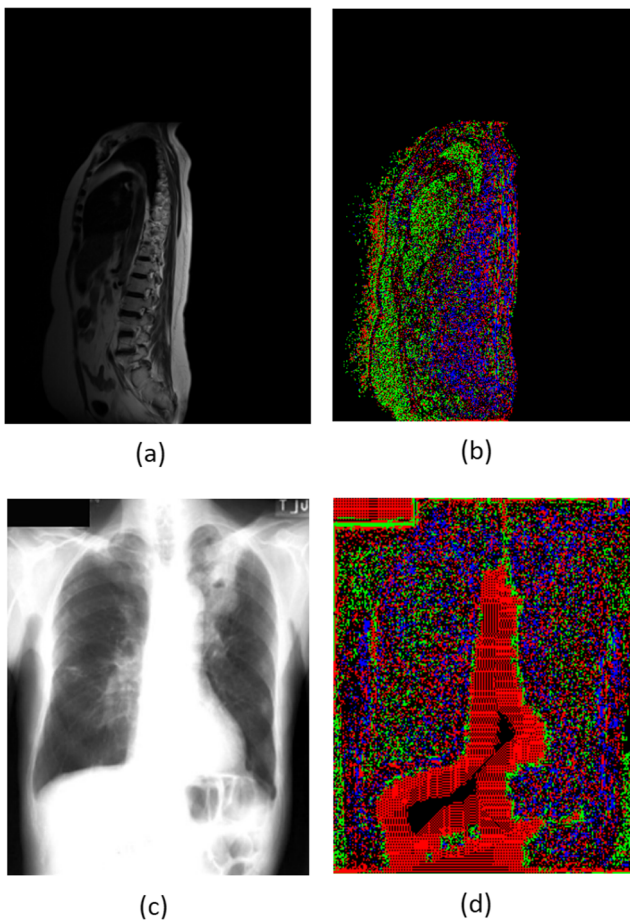


Figure 6 Allocation of the adequate expansion techniques on blocks, **a** Watermarked reduced MR image, **b** Inset mark on MR image, **c** Watermarked reduced CR image, **d** Inset mark on CR image.

calculate the intensities of all the unknown pixels in the expanded image. Therefore, each estimated pixel could have four possible values depending on the used expansion function. Subsequently, each block could have four estimations. To compare each block of the original image with its expected counterpart after reduction / expansion, we used the PSNR metric.

This comparison enabled us to set a selection matrix that allows the identification of the most appropriate expansion function for each block. Since there were 4 expansion techniques, two bits were needed to encode each expansion technique. The values ‘00’, ‘01’, ‘10’ and ‘11’ were adopted to

Table 5 NBpP of a watermarked reduced image using the n^{th} level of wREPro and lossless image compression.

	MR image file formats			CR image file formats		
	BMP	TIFF	JLS	BMP	TIFF	JLS
wREPro level 1	2.03	1.03	0.62	2.03	1.61	0.63
wREPro level 2	0.53	0.29	0.18	0.53	0.48	0.2
wREPro level 3	0.15	0.074	0.046	0.15	0.12	0.06

Table 6 Quality assessment of MR images treated by wREPro at level n in terms of PSNR_{average}(dB).

		$E_W(E_1)^{n-1}$	$E_W(E_2)^{n-1}$	$E_W(E_3)^{n-1}$	$E_W(E_4)^{n-1}$	E_W^n
wREPro	n = 1	50,60	50,60	50,60	50,60	50,60
level n	n = 2	39,84	39,61	35,64	38,80	38,94
	n = 3	32,28	32,25	29,39	32,02	31,41

represent the cardinal sine interpolation, nearest-neighbor interpolation, cubic interpolation and cardinal spline interpolation, respectively. We inserted one of these codes into the least significant bits of the preserved pixels before image transmission.

Upon reception, the receiver extracted the embedded information located in each pixel. Thus, it could recognize the most appropriate expansion technique to use in order to estimate each expanded block.

Hence, the enlarged image was simply a combination of four expansions of the reduced watermarked image. This fusion was realized by the blind watermarking.

We attested that our approach based on image size reduction and watermarking ensured a minimization of the image volume to the quarter which was equivalent to a Number of Bits per Pixel (NBpP) equal to 2 (8bits/4) for grayscale images and equal to 6 (24bits/4) for color images. To further decrease these obtained NBpPs, we suggested to compress the watermarked reduced image by TIFF or JLS lossless compressions. Consequently, before its display, the image had to be decompressed then enlarged as described in Fig. 5.

Where Iorig is the original image, IR is the reduced image (obtained by a square-square mesh decimation), $IRE_{1,2,3,4}$ are 4 reduced then expanded images $\{IRE_1, IRE_2, IRE_3 \text{ and } IRE_4\}$ which are computed by the expansion of IR using respectively E_1, E_2, E_3 and E_4 . IwR is the watermarked reduced image, $IwRE_{1,2,3,4}$ are 4 expanded images $\{IwRE_1, IwRE_2, IwRE_3 \text{ and } IwRE_4\}$ of IwR using respectively E_1, E_2, E_3 and E_4 . IwRE is the fusion of $\{IwRE_1, IwRE_2, IwRE_3 \text{ and } IwRE_4\}$ according to the extracted watermark.

3.3 The n^{th} Level of wREPro

The application of TIFF or JLS compression on an image provided a new fixed-size file because these two methods

Table 7 Quality assessment of MR images treated by wREPro at level n using SSIM_{average}.

		$E_W(E_1)^{n-1}$	$E_W(E_2)^{n-1}$	$E_W(E_3)^{n-1}$	$E_W(E_4)^{n-1}$	E_W^n
wREPro	n = 1	0.9989	0.9989	0.9989	0.9989	0.9989
level n	n = 2	0.9823	0.9810	0.9775	0.9789	0.9784
	n = 3	0.9118	0.9115	0.8848	0.9094	0.9007

Table 8 Quality assessment of CR images treated by wREPro at level n using PSNR_{average}(dB).

		$E_W(E_1)^{n-1}$	$E_W(E_2)^{n-1}$	$E_W(E_3)^{n-1}$	$E_W(E_4)^{n-1}$	E_W^n
wREPro level	n = 1	51,25	51,25	51,25	51,25	51,25
n	n = 2	34,74	34,86	39,52	34,2	42,95
	n = 3	29,08	29,24	30,51	28,69	34,47

are lossless. This prevented us to reduce more the size of the image to transmit or to archive. On the other hand, wREPro could act on the pixels' number of the reduced image and then allowed us to control the size of the image file. The idea was to apply a recursive reduction of the original image. Thus a reduction at level 1 reduced the number of pixels by a factor of 2^1 . To further minimize the image by a factor equal to 2^2 , the reduction occurred at level 2. After repeating these iterations, we obtained a reduction of the original image by a factor of 2^n at level n. When we applied wREPro at level n, the watermarking was done on the image obtained at level n (original image reduced by a factor of 2^n) according to the image of level (n-1) (original image reduced by a factor of $2^{(n-1)}$). We note that level 0 provided us with an image having the same dimensions as the original image.

4 Results and Discussion

In the experimental study, the reduction of the image was carried out using a square-square Mesh method. As for the expansion phase, it involved four techniques, namely B-spline interpolation function, cubic Interpolation, nearest-neighbor interpolation and zero-padding, that we named E_1 , E_2 , E_3 and E_4 , respectively.

We combined the image reduction R with each one of the expansion techniques to get 4 versions of REPro named RE_1 , RE_2 , RE_3 and RE_4 . Profiting from the image watermarking and REPro, we got wREPro (RE_w).

To highlight the effect of watermarking on our proposed compression approaches, we compared the performances of the 4 versions of REPro (RE_1 , RE_2 , RE_3 and RE_4) with those of RE_w .

We carried out our experiments on two medical image databases. The first database was composed of 30 Magnetic

Table 9 Quality assessment of CR images treated by wREPro at level n using SSIM_{average}.

		$E_W(E_1)^{n-1}$	$E_W(E_2)^{n-1}$	$E_W(E_3)^{n-1}$	$E_W(E_4)^{n-1}$	E_W^n
wREPro	n = 1	0.9992	0.9992	0.9992	0.9992	0.9992
level n	n = 2	0.9848	0.9850	0.9864	0.9837	0.9884
	n = 3	0.9529	0.9548	0.9557	0.9240	0.9673

Resonance images (MR) and the second one was formed of 30 Computed Radiography images (CR).

Tables 3 and 4 illustrated the PSNR and SSIM averages assessing the fidelity degrees between each original image (MR or CR) and its reduced then enlarged counterpart using the five studied techniques.

As a matter of fact, the evaluation by PSNR and SSIM averages might not reflect the actual performances of the different techniques. The reduction-expansion technique was denoted as "Selected" if it provided the best similitude between both the original and reduced-expanded images while comparing its performance to the other analyzed techniques. The acquired results in this stage showed that wREPro guaranteed better preservation of the original image quality for all tested medical images according to the PSNR and SSIM metrics. Actually, even if a technique was efficient to expand the whole image, it was not necessarily the case for its components or blocks. Therefore, we noted that wREPro took advantage of E_1 , E_2 , E_3 and E_4 by selecting the best expansion method for each block.

On another hand, Fig. 6a and c showed respectively watermarked reduced MR and CR samples. Each pixel of these images included the label of the selected expansion method to be used. The set of labels formed the signature. As regards Fig. 6b, d, they illustrated the signature embedded in the reduced test images. The Black, Red, Green and Blue colors referred to the RE_1 , RE_2 , RE_3 and RE_4 techniques representing the insertion of '00', '01', '10' and '11' bits respectively. According to these watermarks, it was obvious that different expansion techniques were adopted to generate the final expanded image.

The aim of our wREPro approach was to reduce the image volume to transmit or to archive. Therefore, the NBpP had a great impact on the performance of the compression methods. We note that an image was represented by the quarter of its pixels number when wREPro was at level 1. Subsequently, the NBpP of a grayscale image was equal to 2. Considering the fact that the adoption of the BMP file format needed to insert a header in the archived or transmitted image file, the NBpP became equal to 2.03. To further reduce the watermarked reduced image, we applied the TIFF and JLS lossless image compression.

Moreover, we used the n^{th} level of the wREPro which further decreased the number of pixels of the processed image and yields to a lower NBpP. In this context, we focused on wREPro at levels 1, 2 and 3 which respectively reduced the image size to the quarter, the 16th and the 64th levels. The watermarked reduced image would then be archived or transmitted using the BMP, TIFF or JLS image file format.

According to Table 5 which summarized the obtained NBpP of these combinations, we note that the adoption of JLS lossless image compression ensured the best image volume reduction followed by TIFF and BMP image file formats.

However, a good image compression method should ensure in addition to a high compression rate (low NBpP) a maximum

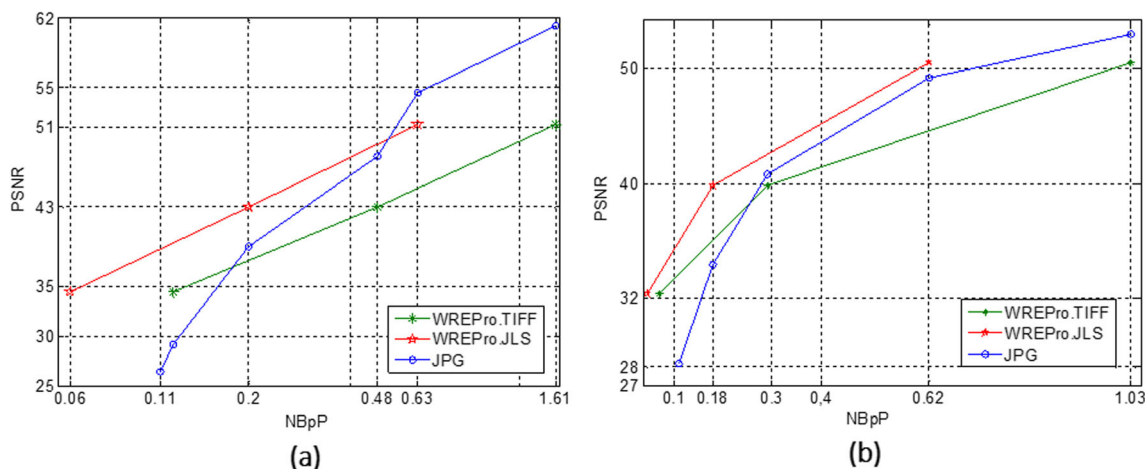


Figure 7 Evaluation of the performances of wREPro.TIFF, wREPro.JLS and JPEG in terms of PSNR. **a** NBpP_{average} versus PSNR_{average} for CR images. **b** NBpP_{average} versus PSNR_{average} for MR images.

of image quality preservation. Thus, we used PSNR and SSIM metrics to compare the original image with the watermarked reduced compressed then decompressed enlarged image. As previously defined and according to Tables 3 and 4, the application of wREPro ensured a maximum of image preservation when it was performed for a single level transition. In other words, wREPro at level n guaranteed the best reconstruction of one image already reduced by REPro at level $n-1$.

Consequently, we could not ensure that watermarking the reduced image by wREPro at level n gave us a maximum fidelity between the enlarged image at level 0 (which had the same size of the original image) and the original image. Hence, we suggested to enlarge the watermarked reduced image at level n by E_w to obtain the best reduced image at level $(n-1)$. Then, we tried to determine from $\{E_1, E_2, E_3, E_4, E_w\}$ the best method of image expansion for (level $(n-1)$ to level 1). The obtained results related to the evaluation studies performed on CR and MR image were illustrated in Tables 6, 7, 8 and 9.

Analyzing these results, we admit that the watermarking guaranteed a better expansion for reduced CR images. However, it is advisable to consider the watermark only in the first transition (n^{th} level to $n-1^{th}$ level) and adopt the B-spline function interpolation in the other following transitions in order to ensure better quality preservation for the reduced MR images.

In terms of the results, we could rule out the use of BMP method for archiving and transmission due to the large volume it causes. Thus, we kept the JLS and the TIFF formats to encode the reduced image. Using such lossless compression methods enabled us to preserve the inserted mark. This embedded information into the reduced image at level n was exploited to reproduce one CR image which was similar to the original one.

However, this marking was exploited to enlarge the MR image from level n to only level $n-1$ while the following image expansions were provided by the B-spline interpolation to ensure a better MR image reproduction.

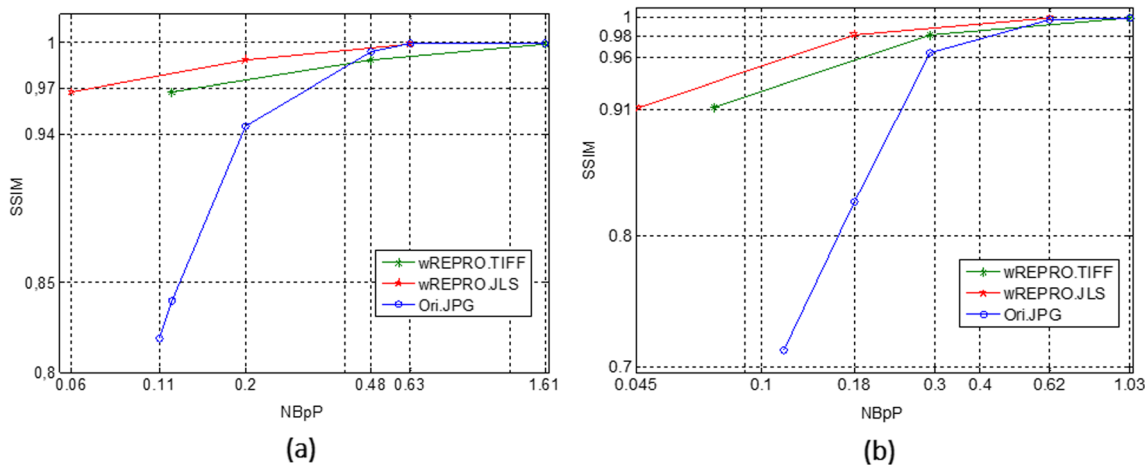


Figure 8 Evaluation of the performances of wREPro.TIFF, wREPro.JLS and JPEG in terms of SSIM. **a** NBpP_{average} versus SSIM_{average} for CR images. **b** NBpP_{average} versus SSIM_{average} for MR images.

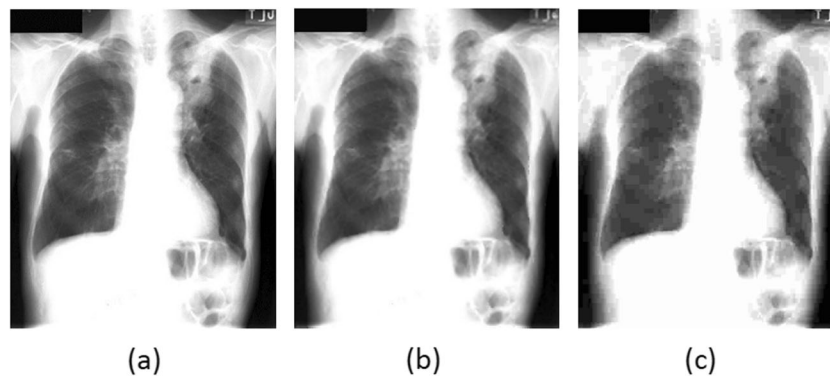


Figure 9 Visual impact of the application of wREPro.JLS at level 4 and JPEG compression on CR Images. **a** Original CR image (NBpP = 8), **b** CR image compressed by wREPro.JLS (PSNR = 35.84 dB,

SSIM = 0.986 and NBpP = 0.18), **c** CR image compressed by JPEG (PSNR = 32.33 dB, SSIM = 0.916 and NBpP = 0.18).

Nevertheless, it was necessary to compare the performances of our wREPro compression approach with those of the JPEG compression in terms of compression ratio and image quality preservation.

Figure 7a and b illustrate the obtained results of this comparison in terms of $PSNR_{average}$ versus $NBpP_{average}$ and in terms of $SSIM_{average}$ versus $NBpP_{average}$ (Fig. 8a and b), for CR and MR images. The blue, green and red curves represent the performances of JPEG compression, wREPro.JLS and wREPro.TIFF respectively.

According to these results, we note that wREPro.JLS ensured better compression rate and image quality compared to wREPro.TIFF. While comparing the performances of wREPro.JLS with those of JPEG applied on MR images, we note that wREPro.JLS preserved better image quality when NBpP is lower than 0.62. Beyond this last NBpP value, the application of JPEG compression led to better results. As for CR images, wREPro.JLS was more efficient than the JPEG compression for low NBpPs. In this case, the NBpP threshold increased from 0.62 to 0.63.

The good performances of wREPro.JLS at high compression ratios were confirmed visually for CR and MR images as illustrated in Figs. 9 and 10. Indeed, compressed CR images (Fig. 9) having one NBpP equal to 0.18 showed better preservation of image quality when processed by wREPro.JLS (PSNR = 35.84 dB and SSIM = 0.986) than by JPEG (PSNR = 32.33 dB and SSIM = 0.916).

Similarly, when the NBpP was equal to 0.1, we proved that our proposed compression method applied on MR images (Fig. 10) caused a distortion lower than the one yielded by the JPEG compression use. Indeed, in this case, our approach provided PSNR = 41.28 dB and SSIM = 0.995, whereas the JPEG method showed PSNR = 30.02 dB and SSIM = 0.751.

5 Conclusion

The main interest of this paper is to ensure a high compression rate for both MR and CR image while guaranteeing a good preservation of the image quality. This leads to reduce the

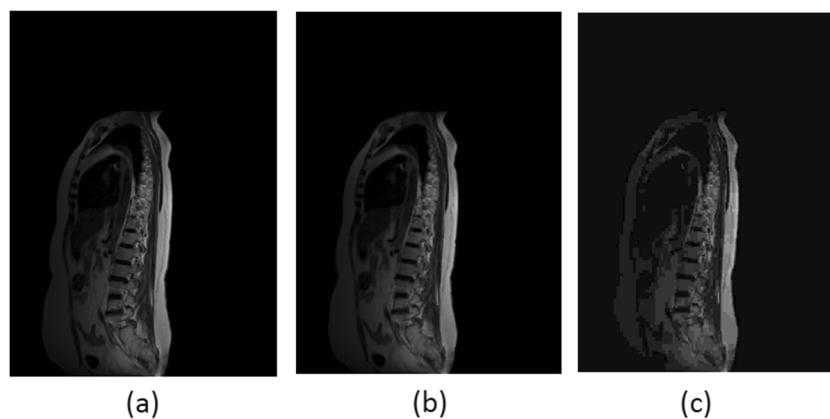


Figure 10 Visual impact of the application of wREPro.JLS at level 4 and JPEG compression on MR Images. **a** Original MR image (NBpP = 8), **b** MR image compressed by wREPro.JLS (PSNR = 41.28 dB,

SSIM = 0.995 and NBpP = 0.1), **c** MR image compressed by JPEG (PSNR = 30.02 dB, SSIM = 0.751 and NBpP = 0.1).

archiving volume of medical images and to facilitate their transmission in a telemedicine application. Unlike the JPEG compression standard which is based on encoding algorithms, our proposed approach combines reduction of the image size and encoding algorithms used for lossless image compression.

To do so, we used the square-square decimation in the compression step and four expansion techniques that are “zero-padding”, “nearest neighbor interpolation”, “cubic interpolation” and “transformed B-Spline” in the decompression step.

To exploit the advantages of each image magnification method, we subdivided the image into 2x2 pixel blocks. Then, we inserted in each pixel the code of its adequate expansion technique. Moreover, we used TIFF and JLS compressions to improve the image compression rate while preserving the watermark. Indeed, the proposed approaches namely wREPro.TIFF (watermarked Reduction / Expansion Protocol combined with TIFF compression) and wREPro.JLS (watermarked Reduction / Expansion Protocol combined with JLS compression) consist in reducing the image, watermarking it, then compressing the resulted image. Compared to the JPEG compression, we notice that wREPro.JLS have ensured a better preservation of the image quality at low NBpPs. Despite their small volumes, the compressed images using wREPro.JLS allowed a right diagnosis due to their high similarity to original images.

We are currently developing a software component that will be integrated into a test version of a diagnostic platform COVOTEM commercialized by Interactive Covalia. In this new phase, we will test various limitations of bandwidth shared by a number of doctors using videoconferencing.

Acknowledgments The authors would like to thank the European Union for financing this project as part of the servastic INTERREGIV program in collaboration with Swiss partners (Vaud University Hospital at Lausanne, and EPFL Lausanne) as well as Sfax and Besancon Universities for their agreement to allow the development of this transversal research work.

References

- Fuin, D., Garcia, E., Guyennet, H., Lapayre, J.C. (2008). Collaborative interactions for medical e-Diagnosis. In *HPCN. Int. Journal on High-Performance Computing and Networking*, 5:189–197.
- Pieralli, C., Wacogne, B., Bonnans, V., Humbert, P., Pazart, L., Marzani, F., Lapayre, J.-C., Lang, C. (2009). Collaborative platform for skin cancer screening and associated optical fibered probe for diagnosis. Proc. Sin'Fran09, Singaporean-French IPAL Symposium, pp 44–55, World Scientific Publishing.
- Xia, Q., Ni, J., Ansuura, J, Gee, J. C. (2015). Searchable public-key encryption with data sharing in dynamic groups for mobile cloud storage. *Journal of Universal Computer Science*, 21(3).
- Chaabouni, I., Fourati, W., Bouhleb, M. S. (2016). Using ROI with ISOM compression to medical image. *Int. J. Computational Vision and Robotics*, 6(1/2).
- Suruliandi, A., Raja, S. P. (2015). Empirical evaluation of EZW and other encoding techniques in the wavelet-based image compression domain. *International Journal of Wavelets, Multiresolution and Information Processing*, 13(02).
- Ang, B. H., Sheikh, U. U., & Marsono, M. N. (2015). 2-D DWT system architecture for image compression. *Journal of Signal Processing Systems*, 78(2), 131–137.
- Bhavani, S., & Thanushkodi, K. G. (2013). Comparison of fractal coding methods for medical image compression. *IET Image Processing*, 7(7), 686–693.
- Doukas, C., & Maglogiannis, I. (2007). Region of interest coding techniques for medical image compression. *IEEE Engineering in Medicine and Biology Magazine*, 26(5), 29.
- Hernández-Cabronero, M., Blanes I., Pinho, A. J., Marcellin, M. W., Serra-Sagristá, J. (2016). Progressive lossy-to-lossless compression of DNA microarray images. *IEEE Signal Processing Letters*, 23(5).
- Castiglione, A., Pizzolante, R., De Santis, A., Carpentieri, B., Castiglione, A., & Palmieri, F. (2015). Cloud-based adaptive compression and secure management services for 3D healthcare data. *Elsevier; Future Generation Computer Systems*, 43–44, 120–134.
- Pizzolante, R., Carpentieri, B., Castiglione, A. (2013). A secure low complexity approach for compression and transmission of 3-D medical images. 2013 Eighth International Conference on Broadband, Wireless Computing, Communication and Applications, pp. 387–392.
- Shih, F. Y., & Wu, Y.-T. (2005). Robust watermarking and compression for medical images based on genetic algorithms. *Medical Image Processing, Information Sciences*, 175(3), 200–216.
- Pu, L., Marcellin, M. W., Bilgin A., Ashok, A. (2015). Compression based on a joint task-specific information metric. 2015 Data Compression Conference
- Ciznicki, M., Kurowski, K., Plaza, A. (2012). Graphics processing unit implementation of JPEG2000 for hyperspectral image compression. *SPIE, Journal of Applied Remote Sensing*, 6(1).
- Bruylants, T., Munteanu, A., & Schelkens, P. (2015). Wavelet based volumetric medical image compression. *Signal Processing: Image Communication*, 31, 112–133.
- Starosolski, R. (2014). New simple and efficient color space transformations for lossless image compression. *Elsevier; Journal of Visual Communication and Image Representation*, 25(5), 1056–1063.
- Wu, X., Li, Y., Liu, K., et al. (2014) Massive parallel implementation of JPEG2000 decoding algorithm with multi-GPUs. Proc. SPIE 9124, Satellite Data Compression, Communications, and Processing X, 91240S.
- Blinder, D., Bruylants, T., Ottevaere, H., Munteanu, A., & Schelkens, P. (2014). JPEG 2000-based compression of fringe patterns for digital holographic microscopy. *Optical Engineering*, 53(12), 14.
- Chemak, C., Lapayre, J.-C., & Bouhleb, M.-S. (2008). Neurology diagnostics security and terminal adaptation for PocketNeuro Project. *International Journal of Telemedicine and e-Health*, 14(7), 671–678.
- Masmoudi, A., Puech, W., Bouhleb, M. S. (2010). Efficient adaptive arithmetic coding based on updated probability distribution for lossless image compression. *Journal of Electronic Imaging*, 19 (2).
- Tan, C. K., Ng, J. C., Xu, X., et al. (2011). Security protection of DICOM medical images using dual-layer reversible watermarking with tamper detection capability. *Journal of Digit Imaging*, 24(3), 528–540.
- Karim, A. M., Khalfallah, A., & Bouhleb, M. S. (2014). A new watermarking technique for medical image using hierarchical encryption. *IJCSI International Journal of Computer Science Issues*, 11(4), 27–32.
- Kallel, M., Bouhleb, M.-S., & Lapayre, J.-C. (2010). Use of multi-watermarking schema to maintain awareness in a teleneurology diagnosis platform. *Radioengineering Journal*, 19(1), 68–73.
- Amri, H., Hanna, F., Lapayre, J.C., Khalfallah, A., Bouhleb, M.S. (2015). REPRO: a new reduction/expansion protocol to increase

- the performance of image transmission in medical telediagnosis platforms. *Biomedical Engineering: Applications, Basis and Communications*, 27(06).
25. Chemak, C., Lapayre, J. C., & Bouhleb, M. S. (2007). New watermarking scheme for security and transmission of medical images for pocket neuro project. *Radioengineering, Special Issue: Advanced Digital Signal Processing*, 16(4), 58–63.
 26. Ogawa Y., Ariki, Y., Takiguchi, T. (2012). Super-resolution by Gmm based conversion using self-reduction image. 37th International Conference on Acoustics, Speech, and Signal Processing ICASSP-2012. Kyoto, Japan, 2012, pp. 1285–1288.
 27. Cruz-Roldána, F., Blanco-Velasco, M., & Godino Llorenteb, J. I. (2012). Zero-padding or cyclic prefix for MDFT-based filter bank multicarrier communications. *Signal Processing*, 92(7), 1646–1657.
 28. Bozek J., Grgic, M., Delac, K. (2010) Comparative analysis of interpolation methods for bilateral asymmetry. 52nd International Symposium ELMAR-2010, 15–17 September 2010, Zadar, Croatia, 2010, pp. 1–7.
 29. Wang, X., Ding, Y., Liu, M.-y., & Yan, X.-l. (2011). Efficient implementation of a cubic-convolution based image scaling engine. *Journal of Zhejiang University Science C*, 12(9), 743–753.
 30. Ruijters, D., & Thévenaz, P. (2012). GPU prefilter for accurate cubic B-spline interpolation. *The Computer Journal*, 55(1), 15–20.
 31. Unser, M., Aldroubi, A., & Eden, M. (1993). B-spline signal processing: Part II - efficient design and applications. *IEEE Transactions on Signal Processing*, 41(2), 834–848.
 32. Thévenaz, P. (2000). Interpolation revisited. *IEEE Transactions On Medical Imaging*, 19(7), 739–758.
 33. Shin, D. K., & Moon, Y. S. (2015). Super-resolution image reconstruction using wavelet based patch and discrete wavelet transform. *Journal of Signal Processing Systems*, 81(1), 71–81.
 34. Vargas-Vera, M. (2015). A framework for extraction of relations from text using relational learning and similarity measures. *Journal of Universal Computer Science*, 21(11), 1482–1496.
 35. Mustapha, H., Bachir, B., Thouraya, M-M. (2015) New secure and robust audio watermarking algorithm based on QR factorization in wavelet domain. *International Journal of Wavelets, Multiresolution and Information Processing*, 13(03).
 36. Khalfallah, A., & Bouhleb, M. S. (2011). The impact of the concept of the family relative signatures on the non-blind watermarking in the multiresolution domain using 9/7 and 5/3 wavelets. *International Journal on Information and Communication Technologies*, 4(3), 111–118.
 37. Kammoun, F., Khalfallah, A., & Bouhleb, M. S. (2006). New scheme of digital watermarking using an adaptive embedding strength applied on multiresolution filed by 9/7 wavelet. *Journal of Imaging Systems and Technology*, 16(6), 249–257.
 38. Khalfallah, A., Brahim, K., Olivier, C. (2007). A new approach to encrypted semi-blind watermarking in multiresolution field by 9/7 wavelet. First international conference of E-Medical Systems – Morocco (E-MediSys'07).
 39. Ohura, R., Minamoto, T. (2015). A blind digital image watermarking method based on the dyadic wavelet packet transform and fast interval arithmetic techniques. *International Journal of Wavelets, Multiresolution and Information Processing*, 13(05)
 40. Sanchez Santana, M.-A., Aupet, J.-B., Betbeder, M.-L., Lapayre, J.-C., & Camarena, A. (2013). A tool for telediagnosis of cardiovascular diseases in a collaborative and adaptive approach. *Journal of Universal Computer Science*, 19(9), 1275–1294.
 41. Kassab, R., Lapayre, J.-C., Aupet, J.-B., Marzani, F., & Pieralli, C. (2013). Scars collaborative telediagnosis platform using adaptive image flow. *ICAE, Integrated Computer-Aided Engineering*, 20(1), 3–14.



Hedi Amri was born in Sfax (Tunisia) in October 1982. He received the Diploma of Engineer on Automatic and Informatics from the National Engineering School of Gabes-TUNISIA (ENIG) in 2007 and the Diploma of Master on Automatic and Informatics from the National Engineering School of Sfax-TUNISIA (ENIS) in 2009 and PhD in Informatics in 2014 from both ENIS Tunisia and FEMTO-ST France. Currently, he is a research member in the Research

Unit of Sciences and Technologies of Image and Telecommunications (SETIT) Sfax - Tunisia and at the CNRS FEMTO-ST Institute (Computer Science Dept) in Bourgogne/Franche-Comte University - France. His research interests are medical telediagnosis, telemedicine applications, Biomedical Engineering and image processing. He is member of the organization committee in the international conference: Sciences of Electronic, Technologies of Information and Telecommunication SETIT'09 and SETIT'12.



Ali Khalfallah was born in Rouen (France) in January 1980. He received the Diploma of Engineer on Electricity from the National Engineering School of Sfax-TUNISIA (ENIS) in 2003 and the Diploma of Master on Electronics from the National Engineering School of Sfax-TUNISIA (ENIS) in 2004. He obtained the Doctorate in Electronics. Currently, he is a research member in the Research Unit of Sciences and Technologies of Image and

Telecommunications (SETIT). He is assistant professor in the National School of Electronics and Telecommunication of Sfax-TUNISIA (ENETCOM). His research interests include digital watermarking, cryptography, image fusion, image reduction/expansion and image processing. He is the organization Chairman of the international conference: Sciences of Electronic, Technologies of Information and Telecommunication SETIT'07, SETIT'09 and SETIT'12.



Malek Gargouri was born in Sfax (Tunisia) in December 1984. She obtained the Honours degree in Information Technology in 2007 and the Diploma of Master in the same field in 2012 from the Higher Institute of Informatics and Multimedia of Sfax. Currently, she is a research member in the Research Unit of Sciences and Technologies of Image and Telecommunications (SETIT) Sfax - Tunisia and in the Laboratory of LIRIS, UMR 5205

CNRS Central School of Lyon, University of Lyon, 36, av Guy de Collongue, F-69134 LYON-ECULLY Cedex, FRANCE. Her research interests include digital watermarking, cryptography, image fusion, image expansion and image processing.



Naima Nebhani was born in Medenine (Tunisia). She received the diploma of a Master of Science degree (Master on computer science) from the University of Sfax, Tunisia, in 2012. Currently, she is a research member in the Research Unit of Sciences and Technologies of Image and Telecommunications (SETIT) Sfax - Tunisia and at the CNRS FEMTO-ST Institute (Computer Science Dept) in Bourgogne/Franche-Comte University – France. Her research

interests include distributed adaptive teleapplication, and interactions in this kind of distributed systems.



Jean-Christophe Lapayre is Professor at the CNRS FEMTO-ST Institute (Computer Science Dept) in Bourgogne/Franche-Comte University (France) since 2002. He is the Responsible of Distributed Algorithmic for Teleapplications Research Group, and member of the Biom'@x Steering Committee (FEMTO-ST's research axis on biomedical area). His general field is the Distributed Systems and his present research interests are medical telediagnosis and

telemedicine applications. He is the Head of the third year in ISIFC

Biomedical Superior Institute of Engineers of Franche-Comte with a specific e-Health & Telemedicine orientation.



Mohamed Salim Bouhleb was born in Sfax (Tunisia) in December 1955. He is a full professor at Sfax University, Tunisia. He is the Head of the Research Group: Sciences and Technologies of Image and Communication since 2003. He was the director of the Higher Institute of Electronics and Communications of Sfax-TUNISIA (ISECS) 2008–2011. He received the golden medal with the special appreciation of the jury in 1999 on the occasion

of the first International Meeting of Invention, Innovation and Technology (Dubai, UAE). He was the vice president and founder member of the Tunisian Association of the Specialists in Electronics and the Tunisian Association of the Experts in Imagery. He is the president and founder of the Tunisian association on Human-Machine Interaction since 2013. He is the Editor in Chief of the international Journal “Human-Machine Interaction” and a dozen of special issues of international journals. He is the Chairman of many international conferences and member of the program committee of numerous international conferences. His research interests are Image processing, Telecommunication and Human-Machine Interaction in which he has obtained more than 20 patents so far. More than 500 articles were published in international journals, conferences and books. Moreover, he has been the principal investigator and the project manager for several research projects dealing with several topics concerned with his research interests mentioned above.